Hybrid lithium-ion battery and hydrogen energy storage systems for a wind-supplied microgrid

Michael Anthony Giovanniello,[#] Xiao-Yu Wu[*]

Department of Mechanical and Mechatronics Engineering, University of Waterloo, 200 University Avenue West, Waterloo, ON, Canada N2L 3G1

Present address: MIT Energy Initiative, Massachusetts Institute of Technology, 77 Massachusetts Ave, Cambridge, MA 02139, United States

* Corresponding Author's Telephone: Xiao-Yu Wu, +1-519-888-4567 x36849
* Corresponding Author's Email: Xiao-Yu Wu, xiaoyu.wu@uwaterloo.ca

---

Abstract

Microgrids with high shares of variable renewable energy resources, such as wind, experience intermittent and variable electricity generation that causes supply-demand mismatches over multiple timescales. Lithium-ion batteries (LIBs) and hydrogen (H_2) are promising technologies for short- and long-duration energy storage, respectively. A hybrid LIB-H_2 energy storage system could thus offer a more cost-effective and reliable solution to balancing demand in renewable microgrids. Recent literature has modeled these hybrid storage systems; however, it remains unknown how anticipated, but uncertain, cost reductions and performance improvements will impact overall system cost and composition in the long term. Here we developed a mixed integer linear programming (MILP) model for sizing the components (wind turbine, electrolyser, fuel cell, hydrogen storage, and lithium-ion battery) of a 100% wind-supplied microgrid in Canada. Compared to using just LIB or H_2 alone for energy storage, the hybrid storage system was found to provide significant cost reductions. A sensitivity analysis showed that components of the H_2 subsystem meaningfully impact the total microgrid cost, while the impact of the LIB subsystem is dominated by its energy storage capacity costs. As technologies evolve, the H_2 subsystem assumes a greater role (i.e., it is larger and receives/supplies more energy over more hours) compared to the LIB subsystem, but LIB continues to provide frequent intra-day balancing in the microgrid.

Highlights

- Hybrid LIB-H_2 storage achieves lower cost of wind-supplied microgrid than single storage
- LIB provides frequent intra-day load balancing, H_2 is deployed to overcome seasonal supply-demand bottlenecks
- By 2050, the role of H_2 relative to LIB increases, but LIB remains important
- System cost is sensitive to the cost of all H_2 components and LIB energy storage capacity cost

---

Keywords

Hydrogen, lithium-ion battery, energy storage, hybrid storage, microgrid, wind energy, renewables, energy optimization

Nomenclature

Abbreviations	
AC	Annualized cost
CAPEX	Capital Expenditure
El	Electrolyzer
FC	Fuel cell
H_2	Hydrogen
HS	Hydrogen storage
LIB	Lithium-ion battery
LIB_E	Lithium-ion battery energy
LIB_P	Lithium-ion battery power
LT	Project or technology lifetime
MILP	Mixed-integer linear programming
OPEX	Operating Expenditure
SL	Single-layer
SOC	State of charge
TL	Two-layer
Indices	
$t \in T$	Index of 8,760 hours in a year
Parameters	
$Cost_{AC,i}$	Annualized cost of component i
$Cost_{AC,System}$	Total annualized cost of the microgrid
$D(t)$	Energy demand at hour t
Eff_i	Efficiency of component i
Min/Max_SOC_i	Minimum/maximum state of charge of component i
$P_{Tu}(t)$	Energy produced by one turbine at hour t
Variables	
Cap_i	Capacity of component i (component capacities are positive continuous variables, except Cap_{Tu} which is an integer variable representing the number of turbines)
$E_i(t)$	Energy stored in storage component i at hour t
$lb_{1,2,3,4,5}$	Binary variables used to choose the LIB energy-power ratio
M	An arbitrary constant
$P_i(t)$	Power input/output by component i at hour t
$ub_{1,2,3,4,5}$	Binary variables used to choose the LIB energy-power ratio
$y_{1,2}$	Binary variables that prohibit simultaneous LIB charge and discharge

1 Introduction

Microgrids, which currently provide electricity to 47 million people across 134 countries and territories, are likely to play an increasing role in future power systems. By 2030, the World Bank estimates that an additional 490 million people (of the 1.2 billion who will require electricity access by

then) could be supplied cost-effectively with microgrids. This potential is largely due to dramatic cost reductions for the technologies that comprise "third-generation" microgrids, including distributed renewable energy resources, energy storage, inverters, diesel generators, etc. [1].

Another driver behind microgrid growth is their ability to help power systems mitigate and adapt to climate change. Microgrids support power sector decarbonization by enabling greater deployment of distributed renewable energy resources. They also improve reliability and resilience for their direct end-users and greater power systems, which is becoming especially relevant as climate change increases the frequency and severity of extreme weather events[2]. For these reasons, policymakers are looking towards microgrids as a solution for lowering power sector emissions and bolstering energy security [3], [4] — most notably, the 2022 U.S. Inflation Reduction Act, which significantly expands subsidies/incentives for distributed renewables, energy storage, and microgrid controllers [5].

Historically, diesel generators have been the primary resource for electricity generation in microgrids[6]. And in the third-generation microgrids that the World Bank forecasts will dominate growth going forward, diesel generators continue to play a role due to the intermittent and variable nature of renewable generation. Unfortunately, these diesel generators produce greenhouse gases that undermine the climate benefits of microgrids and air pollutants that have serious health consequences for users [7]. In Canada, where diesel generators supply up to 79% of electricity in remote communities, the federal government has committed $300 million to ensure that all rural, remote, or indigenous communities with diesel generators have the opportunity to switch to clean electricity by 2030 [8].

Energy storage has the potential to eliminate the use of fossil fuel in microgrids and enable reliable, 100%-renewable systems. In addition to periods of underproduction, microgrids with high shares of variable renewables experiences periods of overproduction in which energy is curtailed. Hence, energy storage serves as a bridge between these periods of over- and under-production, ensuring a reliable electricity supply for end users and reducing the uneconomical curtailment of renewable energy. In systems with high shares of renewable, these mismatches take form over multiple timescales, from minutes to years [9]. For example, a 100%-wind supplied microgrid may experience short duration mismatches in which certain hours experience excess or shortfalls, as well as long duration mismatches in which one season experiences overproduction and another underproduction. Therefore, a combination of energy storage technologies suited for storage over different durations may be necessary to ensure reliable, cost-effective operation.

Lithium-ion batteries (LIBs) and hydrogen (H_2) have emerged as leading candidates for short- and long-duration storage, respectively. LIBs are a proven alternative to the traditionally used lead acid batteries, and "should quickly dominate isolated microgrid applications" given expected cost reductions [10]. The components of a H_2 storage system are technologically proven. The International Renewable Energy Agency (IRENA) forecasts up to ~86% for electrolyzers by 2050 [11], and the U.S. DOE has set an ultimate target of 84-88% cost reductions for fuel cells[1] [12]. These dramatic cost reductions are spurred by ambitious nation-level policies, including: 1) the U.S. DOE's *Hydrogen Earth Shot* target for 80% cheaper green H_2 by 2030 [13]; 2) an estimated $13 billion for clean H_2 by 2030 under the *2022 U.S. Inflation Reduction Act* [14]; 3) the European Union's *REPowerEu* target for 10 million tonnes of domestic renewable H_2 production and 10 million tonnes of imported renewable H_2 by 2030 [15]; 4) China's target for 100,000-200,000 tonnes of renewable H_2 by 2025 under the *Medium- and Long-Term Plan for the Development of Hydrogen Energy Industry (2021-2035)* [16].

The key components of a microgrid with hybrid LIB-H_2 storage — electrolyzers, fuel cells, H_2 storage, batteries, and renewables — are expected to experience significant cost reductions and performance improvement in coming decades. But the pace and magnitude remain uncertain. Previous studies have explored the feasibility of such systems; however, to the best of our knowledge, no study has conducted a comprehensive analysis of how cost and efficiency improvements for each component technology will impact total system cost and composition going forward.

[1] The DOE ultimate target is for fuel cells for transportation; however, achieving these targets for transportation applications would likely coincide with cost reduction for stationary applications.

Existing works has explored methods for sizing and operating renewable microgrids with hybrid energy storage[17]. Moretti et al. identified two main categorizes for approaches that have been applied specifically to sizing off-grid hybrid renewable energy microgrids: two-layer (TL) and single-layer (SL) [18]. TL methods are those in which design and operation are decoupled. In TLs, a 'design identification' algorithm generates a solution, which is then passed to a 'dispatch strategy' algorithm that simulates operation and determines operating costs. Based on the 'fitness' of the proposed design solution, a new design solution is proposed, and this process iterates until an optimal solution is found. Hannan et al. [19] and Chauhan and Saini [20] surveyed common TL approaches and provided a list of their application in different studies.

SL methods deal with design and operation simultaneously. SLs typically take the form of mixed integer linear programming (MILP) models, with energy dispatch and component sizes being treated as variables that are jointly solved. Studies comparing TL and SL MILP approaches have found that the SL MILP provides lower cost solutions and improved system performance [18][21]. However, SL MILPs are limited by high computational demands, which increases exponentially with more complex constraints and longer timeseries. In contrast, the lower computational demands of TL methods allow for more detailed models, which can also be non-convex, and therefore require multi-layer approaches [22], [23]. Several methods have been proposed to reduce computation time for intensive SL MILP problems, including iteratively increasing the resolution of input data, aggregating 'typical' timespans, and identifying 'extreme' periods that represent bottlenecks the system is size against [24]–[26].

In this study, we aim to identify which technological advancements (i.e., energy efficiency and cost reduction of different components) yield the greatest benefits for microgrids, and to uncover dynamics in the co-sizing and operation of hybrid energy storage systems and renewable resources. Based on Marocco et al. [21], we developed an SL model for sizing a 100%-wind supplied microgrid with hybrid LIB-H_2 energy storage using a year-long time horizon to account for the season role of H_2 storage with short enough timesteps (i.e., hourly) to account for the short-duration role of LIBs. We compared the hybrid storage system with systems that have just LIB and just H_2 storage to assess the benefits of the hybrid configuration. Then we conducted sensitivity analyses on the effect that individual component cost and efficiency improvements have on system cost and composition.

This study will also contribute to the discussion on hydrogen development in Ontario, Canada and Canada's target of providing clean electricity for remote communities. In April 2022, the government of Ontario released *Ontario's Low-Carbon Hydrogen Strategy: A Path Forward*, detailing the province's ambitions and plans for achieving a "low-carbon hydrogen economy" [27]. The *Strategy* identifies the Greater Toronto Area on its shortlist of possible hydrogen hubs, noting the high concentration of potential hydrogen end-users. Therefore, we have chosen to analyze a hybrid LIB-H_2 storage in the context of a hypothetical residential microgrid in the Greater Toronto Area, using residential demand and wind data from the region. While the present study analyzes a more general system in Ontario, further refinement of the problem statement and model could be used to provide specific and actionable insights for policymakers in other jurisdictions.

2 Methods

2.1 Demand

This paper analyzes a completely grid-isolated microgrid in the Greater Toronto Area that is supplied entirely by wind energy and serves 10,000 residential consumers. A Markov Chain Monte Carlo model, similar to the one presented in Wilke et al. [28], was adopted to simulate the one-year electricity demand data for 1,000 occupants in a medium apartment, which was then scaled to 10,000 consumers. To start, conditional probabilities were generated based on a time use study of ~20,000 people in 2005 in

Canada (obtained from the Centre for Time Use Research [29]), which detailed each participant's activities throughout the day. Then, a Markov Chain Monte Carlo simulation was used to generate hourly appliance use data for 1,000 different people. Power consumption for each appliance was then summed hourly and added to the building's heating/cooling load to create an hourly electricity demand (i.e., power). The simulated hourly power demand data can be found in the supplementary table, which has a similar seasonal change profile with the residential electricity data of the City of Toronto generated by eQUEST [30]. The average annual electricity demand was simulated to be 12,435 kWh/consumer, which is similar to the reported average value of 7,200 – 11,135 kWh/household in Canada (excluding the natural gas use in heating that could accounts for around 63% of annual household energy use) [31].

2.2 Supply

The microgrid is powered by wind energy only. Wind production data was calculated by first simulating one year of hourly wind data with an adapted Markov Process based on 25 years of historic wind data from the region provided by Environment and Climate Change Canada [32]. Historical wind data was sorted by month and hour of the day, and the conditional probabilities of going from one value to another according to month and hour of the day were calculated. Then, the power output of a Vestas V90-2.0 MW turbine was generated using the open source *windpowerlib* Python module, which calculates power output as a function of wind speed using a power curve specific to the turbine [33]. We calculated the output of only one turbine and assumed that all turbines in the wind farm have the same power output. Then the optimal number of turbines was decided by the MILP model described later in the paper. The year-long hourly wind power output can be found in the supplementary file S2. Under the simulated wind profile used in this study, each 2MW turbine produces 5,804 MWh of electricity a year, at a capacity factor of 33.1%.

2.3 Hybrid energy storage system

In the hybrid-storage microgrid analyzed by this study, electricity demand is covered entirely by local wind power resources, while a hybrid LIB-H_2 energy storage system bridges mismatches between wind energy supply and electricity demand. In the H_2 subsystem, electricity is converted to H_2 using a proton exchange membrane (PEM) electrolyzer (El). Hydrogen is kept in a storage system (e.g., above ground tanks in the baseline scenario) and converted back into electricity using a PEM fuel cell (FC). Alongside the H_2 subsystem, there is a LIB subsystem that is modelled using power conversion (LIB_P) and energy storage (LIB_E). The capacities of battery power conversion and energy storage are independent variables, but energy storage capacity is restricted to 2, 4, 6, 8, or 10 times of power conversion capacity, in keeping with National Renewable Energy Laboratory (NREL) Annual Technology Baseline cases for utility scale LIBs [34]. Cost and efficiency parameters of different components in the microgrid in the *2020 Hybrid Base Case* are shown in Table 1, which are consistent with MIT's 2022 "The Future of Energy Storage" study [35]. These parameters are projected to be improved over time, and the improved values in the 2050 Hybrid Case are summarized in Table S1. Table 2 describes additional project parameters used in both the 2020 and 2050 cases.

Table 1: Cost and Efficiency Parameters of different components in the microgrid (2020 Hybrid Base Case)

Technology[a]	Power Conversion CAPEX ($/kW)	Energy Storage CAPEX ($/kWh)	Fixed Operation and Maintenance (FOM)	Replacement Cost[b] ($/kW-year)	Life (years)	Efficiency (%)	Annualized Cost ($/kW or kWh)

			($/kWh-year)				
Electrolyzer[c]	1,785 [36]	-	79.4 [36]	19.9/year [36]	20	58 [35][d]	267.79
Fuel Cell	2,864[37]	-	120.2	31.9/year	20	45 [37]	422.44
H_2 Storage Tank	-	8 [35]	0.08[e]	-	Project Life	96 [38]	0.835
LIB Power Capacity[f]	257	-	1.4	*	10	92, each way [35]	25.66
LIB Energy Capacity	-	277	6.8	*	10	5% (monthly self-discharge rate)[g] [39]	32.95
Turbine[h]	2,924,000/ 2MW turbine	-	86,000	-	25	-	362004.91/ 2MW turbine

[a] Cost parameters from all sources adjusted to 2020 USD using an online inflation adjustment calculator[40].
[b] Following the MIT Future of Energy Storage study [35], replacement costs are accounted for as fixed yearly expenses. Fuel cell fixed operation and maintenance FOM and replacement costs are calculated as a fixed percentage of Capital Expenditure (CAPEX) and assumed the same percentages as the electrolyzer — 4.2% and 1.1%, respectively.
[c] There is an important difference in how we measure power capacity for electrolyzer and fuel cell. For the electrolyzer, we report $/kWe, defined as the maximum power input — for example, running a 100 kWe electrolyzer with efficiency 58% at full capacity for an hour will produce hydrogen with an energy content of 58 kWh. Fuel cell capacity, on the other hand, is defined by the maximum power output. Running a 100kW fuel cell with efficiency 45% at full capacity for an hour will produce 100kWh of electricity and consume 222.2 kWh equivalent of hydrogen.
[d] The MIT Future of Energy Storage study assumes electrolyzer requires 5.2 kWh of electricity per cubic meter of hydrogen, which has an energy equivalent of 3 kWh of electricity, meaning electrolyzer efficiency of ~58%.
[e] It is assumed to be 1% of the CAPEX [41]
[f] LIB power and energy capacity data assume the 2020 current costs from the Future of Energy Storage study [35], which are calculated using data from NREL's 2020 Annual Technology Baseline (ATB) for Solar PV and Energy Storage [42]. FOM costs include replacement due to degradation.
[g] 5% monthly self-discharge (95% efficiency) corresponds to a 0.999929% hourly efficiency, which is the value passed to the model.
[h] Turbine parameters are from NREL's 2020 Wind ATB [43].

Table 2: Project Parameters used to calculate the system cost

Lifetime (years)	20
Nominal Discount Rate	0.07
Capitol Recovery Factor	0.0858

3 Methodology

Figure 1 outlines each step of the methodology. First, we compiled the input data, including technology parameters (cost, efficiency, lifetime, etc.), hourly windspeed data, and hourly power demand data. Then, we processed the data to produce the model inputs, including annualized technology costs, the hourly power output of one turbine, and hourly load. This data was input to a sizing model (Step 1 - Sizing MILP) that return the most cost-effective system configuration. This configuration (i.e., component sizes) is then passed as a set of fixed parameters to a second operation model (Step 2 - Operation MILP) that generates an updated (i.e., improved) hourly operation profile. Figure 1 illustrates these steps and the relationship between the sizing model and operation model.

The Step 1 sizing model is a single-layer mixed integer linear programming (SL-MILP) model that finds the least cost configuration of the wind-supplied microgrid with hybrid LIB-H_2 energy storage. It minimizes the total system cost subject to the constraints described in the following sections. The decision variables are the sizes of the components of the microgrid (i.e., electrolyzer, fuel cell, H_2 storage tanks, LIB power, LIB energy storage, and wind turbines). This model deals with sizing of the components alongside managing hourly energy flows. Constraints are imposed to ensure that all load is met all the time, and that the power flowing through/the energy stored in each component cannot exceed that component's power/energy capacity.

The Step 2 operation model is an adaptation of the Step 1 model that generates an updated operation profile. This model returns hourly power flows to and from both energy storage subsystems, as well as initial states of charge (SOC) of both subsystems. A new objective is implemented to maximize the sum of energy stored in both subsystems over the year. Operating constraints are the same as Step 1, but component capacities are now fixed parameters set according to the results of Step 1.

Step 2 is necessary because under Step 1 only the bare minimum amount of energy required to make it through bottlenecks (i.e., the times with the largest difference between power demand and wind power generation) is stored. By altering the objective function to maximize for energy stored, Step 2 guarantees that excess energy is stored whenever possible, which is closer to the actual operation of an energy storage system. Note that the Step 1 sizing remains cost optimal for Step 1, because the system is still influenced by the same bottlenecks — all that is changed is that the objective is rewarded for keeping storage levels as high as possible. The energy flows returned by Step 2 are analyzed to understand roles and interplay of the two storage subsystems in the yearly operation.

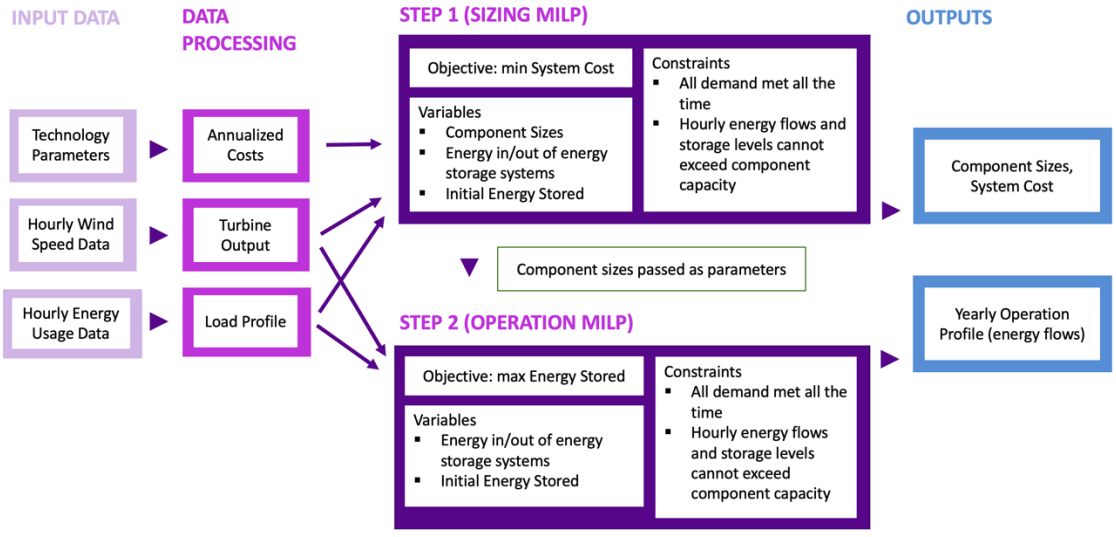

Figure 1: Methodology Overview.

3.1 Cost-Based Objective Function

The objective function in Step 1 minimizes for total annualized system cost, $Cost_{AC,System}$ (2020 USD), which is defined as the sum of the annualized costs of each component technology, $Cost_{AC,i}$, multiplied by that component's capacity, Cap_i.

$$Cost_{AC,System} = \sum_i Cost_{AC,i} * Cap_i \quad (1)$$

Here, *i* is the components in the microgrid system. The annualized cost of a component is the cost it incurs over its lifetime spread equally over every year of the project lifetime. In this study, the annualized cost accounts for the initial capital expenditure (CAPEX), operating expenditure (OPEX, comprised of operation and maintenance costs and replacement costs), and salvage value[2]. Component lifetimes are assumed to be fixed (shown in Table 1), as opposed to dynamic (i.e., dependent on system operation). Annualized cost is calculated as:

$$Cost_{AC,i} = CFR * NPC \quad (2)$$

where CFR is the capital recovery factor, a ratio used to represent the present value of an asset in the future, and *NPC* is the net present cost, a tally of all expenses and the salvage value associated with a component over the project that is adjusted to the current currency. The exact process followed for calculating NPC can be found on the HOMER webpage [44]. CFR is calculated using the real annual discount rate, *dr*, and the project lifetime, $LT_{Project}$, as:

$$CFR(dr, LT_{Project}) = \frac{dr\ (1+dr)^{LT_{Project}}}{(1+dr)^{LT_{Project}} - 1} \quad (3)$$

3.2 Demand Balancing Constraint

A constraint is imposed to guarantee that all power demand is met all the time:

$$Cap_{Tu} * P_{Tu}(t) - P_{El}(t) - P_{LIB,in}(t) - P_{Ct}(t) = D(t) - Eff_{FC} * P_{FC}(t) - Eff_{LIB} * P_{LIB,out}(t) \quad (4)$$

where Cap_{Tu} is the number of turbines, $P_{Tu}(t)$ is the power output of one turbine, $D(t)$ is the power demand of the microgrid community, and $P_{Ct}(t)$ is the amount of curtailed power at time *t*. *Eff* is the power efficiency of each component.

3.3 Component Power Conversion Capacity Constraints

[2] Salvage value allows for more balanced assessment of cost by accounting for the fact that the lifetimes of different components will align different with project lifetime. In the case this study's 20-year project, given a 25-year turbine lifetime and no salvage value, the annualized cost for turbines will include 5 years of unused asset life. On the other hand, the fuel cell (20-year system life) and battery (10-year replacement cycle) will have no unused value by the end of the project. Factoring in salvage value reduces the penalty arbitrarily imposed on turbines for having a replacement schedule that is misaligned with project life.

Power conversion constraints ensure that the power outputs of each energy conversion component (battery, electrolyzer, fuel cell) do not exceed their power conversion capacity, *Cap*.

3.3.1 LIB Subsystem Power Conversion Capacity Constraints

Battery power capacity is defined as the maximum power input when charging or discharging. The usable energy charged or discharged is defined as $Eff_{LIB} * P_{LIB,in/out}(t)$. Battery charging (in) and discharging (out) power constraints are:

$$P_{LIB,in}(t) \leq Cap_{LIB\_P} \quad (5)$$

$$P_{LIB,out}(t) \leq Cap_{LIB\_P} \quad (6)$$

where $P_{LIB,in}(t)$ is power used for charging and $P_{LIB,out}(t)$ is power used for discharging (both as defined as positive real numbers).

Since the LIB subsystem cannot physically charge and discharge simultaneously, two constraints were included to forbid simultaneous battery charging and discharging. To formulate these constraints, we introduce two vectors of binary variables, $y_1(t)$ and $y_2(t)$, and a constant, M, which is set to be greater than the maximum possible value of $P_{LIB,In}(t)$ or $P_{LIB,Out}(t)$ for all t. For the following constraints to work, M must be greater than all possible values of $P_{LIB,in/out}(t)$, which cannot exceed maximum power demand or maximum turbine capacity. Since the maximum power demand is 33MW, and it was assumed that turbine capacity was highly unlikely to exceed 15 times of the maximum demand, M was arbitrarily set to 500.

$$P_{LIB,In}(t) - y_1(t) * M \leq 0 \quad (7)$$

$$P_{LIB,Out}(t) - y_2(t) * M \leq 0 \quad (8)$$

$$y_1(t) + y_2(t) \leq 1 \quad (9)$$

The above constraints guarantee that at least one of $P_{LIB,In}(t) \leq 0$ or $P_{LIB,Out}(t) \leq 0$ is true for all hours t, making simultaneous charge and discharge impossible (since $P_{LIB,In/Out}$ are positive real numbers, this constraint sets at least one equal to 0). However, the same constraints were not imposed on the H_2 subsystem, because the fuel cell and electrolyzer are separate and can run simultaneously. Regardless, simultaneous operation of the electrolyzer and fuel cell did not occur in any of the cases whose energy flows were carefully analyzed.

The LIB energy-power ratio, *x*, is an integer value (either 2, 4, 6, 8, or 10), as described in Section 2.3. In our model, each *x* has a pair of two constraints (Equations 10 and 11), but only one pair from the five is active, which is what determines the optimized *x* value.

$$Cap_{LIB\_E} - ub_x * M \leq x * Cap_{LIB\_P} \quad (10)$$

$$Cap_{LIB\_E} + lb_x * M \geq x * Cap_{LIB\_P} \quad (11)$$

where $x \in \{2, 4, 6, 8, 10\}$, ub_x and lb_x are sets of binary variables standing for upper bound and lower bound of the LIB energy-power ratio, respectively, and M is an arbitrary constant. By setting M arbitrarily high, we can use ub_x and lb_x to activate or deactivate pairs of constraints. If ub_x and lb_x are 1, the pair of constraints are inactive (these constraints are always met). Setting ub_x and lb_x to 0 activates the constraint pair and the value x of the activated pair will be the optimized LIB energy-power ratio.

Additional constraints were used to guarantee that one and only one pair of energy-power ratio constraints can be active. First, we impose that exactly two of the above constraints must be active (i.e., exactly one of ub_x and one of lb_x is 0).

$$\sum_x ub_x == 4 \tag{12}$$

$$\sum_x lb_x == 4 \tag{13}$$

This final set of constraints ensures that that active constraints are for the same energy-power ratio — e.g., $ub_2 = lb_2 = 0$ would activate the constraints (Equations 10 and 11) that set the lower and upper bounds of the energy-power ratio to 2, so the energy-power ratio equals 2.

$$ub_x == lb_x \tag{14}$$

3.3.2 Hydrogen Subsystem Power Capacity Constraints

Electrolyzer power capacity, Cap_{El}, is defined as the maximum electrical power that the electrolyzer consumes. $P_{El}(t)$ is defined as the power used at time t to produce and store H_2, which includes power consumption for H_2 compression:

$$P_{El}(t) = P_{Electrolysis}(t) + P_{Compression}(t), \tag{15}$$

where $P_{Compression}(t)$ is the power required for H_2 compression, and is a fixed portion $(1 - Eff_{HS})$ of the energy content of the H_2 being stored ($Eff_{El} * P_{Electrolysis}(t)$) in that hour t. Hence, Equation (15) can then be rewritten and simplify as:

$$P_{El}(t) = P_{Electrolysis}(t) + (1 - Eff_{HS}) * \left(Eff_{El} * P_{Electrolysis}(t)\right) \tag{16}$$

Since Cap_{El} is the maximum possible value of $P_{Electrolysis}(t)$, we can substitute Cap_{El} for $P_{Electrolysis}(t)$ to derive the final electrolyzer power capacity constraint as:

$$\frac{P_{El}(t)}{\left(1 + Eff_{El} * (1 - Eff_{HS})\right)} \leq Cap_{El} \tag{17}$$

The capacity of the fuel cell, Cap_{FC}, is defined as its maximum power *output*. $P_{FC}(t)$, the energy power equivalent of the quantity of H_2 consumed by the fuel cell, is thus constrained by the following inequality:

$$P_{FC}(t) * Eff_{FC} \leq Cap_{FC} \quad (18)$$

3.4 Energy Storage Constraints

The quantities of stored energy in the LIB subsystem $E_{LIB}(t)$ and H_2 subsystem $E_{HS}(t)$ at each time *t* are tracked as follows. The storage level at time t is equal to the storage level at time $t-1$ plus the amount entering storage (i.e., the H_2 output by the electrolyzer, or the LIB energy charged) and minus the amount leaving storage (i.e., the H_2 consumed by the fuel cell, or the energy drawn by the LIB).

$$E_{HS}(t) = E_{HS}(t-1) + \left(Eff_{El} * P_{Electrolysis}(t) - P_{FC}(t-1)\right) * 1\ hour, \qquad t \in (2, end) \quad (19)$$

$$E_{LIB}(t) = E_{LIB}(t-1) + \left(Eff_{LIB\_P} * P_{LIB,In}(t-1) - P_{LIB,Out}(t-1)\right) * 1\ hour, \qquad t \in (2, end) \quad (20)$$

Note that these constraints begin at time t = 2. This is because the initial energy stored in both subsystems, $E_{LIB/HS}(1)$, are variables independent of previous energy flows. The model ensures that the final energy storage levels for both the H_2 storage tank and LIB are greater than or equal to their initial energy storage levels, which guarantees sustainability year after year:

$$E_i(1) \leq E_i(end), \qquad i \in \{HS, LIB\} \quad (21)$$

Two additional constraints are imposed on both the LIB and H_2 subsystems to keep energy storage levels within predetermined bounds, defined as fractions of total energy storage capacity (30%-90% for battery, 10.7%-100% for H_2).

$$E_i(t) \geq \text{min\_SOC}_\text{i} * Cap_i, \qquad i \in \{HS, LIB\_E\}, \quad (22)$$

$$E_i(t) \leq \text{max\_SOC}_\text{i} * Cap_i, \qquad i \in \{HS, LIB\_E\} \quad (23)$$

3.5 Sensitivity Analysis

The Step 1 SL MILP was applied to conduct sensitivity analyses on the effect of component cost and efficiency on total system cost and composition. Cases were constructed by incrementally increasing/decreasing the cost of each technology individually as well as the components of the H_2 and LIB subsystems together. Similar sensitivity analyses were conducted for component efficiency.

3.6 Updated Objective Function for Step 2 Operation MILP

The Step 1 sizing MILP is adapted to form the Step 2 operation MILP, which generates an updated operation profile. This model returns hourly power flows to and from both energy storage subsystems, as well as initial state of charge (SOC) of both subsystems. Component capacities determined by Step 1 are passed to Step 2 as fixed parameters, and a new objective is implemented to maximize to sum of energy stored in both subsystems over the year:

$$\max\left(\sum_{t=1}^{8760}\sum_{i} E_i(t)\right), \qquad i \in \{LIB, HS\} \tag{24}$$

4 Results and Discussion

4.1 2020 Hybrid Base Case

Table 3: Composition and Cost Breakdown of the Hybrid-Storage Microgrid, 2020 Hybrid Base Case

	Capacity	Annualize Cost (million USD)
Electrolyzer	15.1 MW	4.8
Fuel Cell	18.7 MW	8.1
H_2 Storage Tank	4883.4 MWh	4.1
LIB Charge/Discharge Power	54.1 MW	1.3
LIB Energy Storage	324.7 MWh	9.7
Wind Farm	84 (42 turbines × 2 MW/ turbine)	15.2

The hybrid microgrid is comprised of the wind farm and the hybrid storage system, which is divided into the LIB and H_2 subsystems. The LIB subsystem consists of LIBs and can be described using LIB power capacity and LIB energy storage capacity. The two parameters are related using the LIB energy-power ratio. The H_2 subsystem is comprised of electrolyzer, fuel cell, and H_2 storage tanks. For simplicity, we use 'subsystems' to refer to the LIB and H_2 subsystems and the wind farm. 'Components' refers to the technologies that comprise these subsystems.

Table 3 reports the most-cost effective composition of the *2020 Hybrid Base Case* (i.e., using the 2020 baselines assumptions reported in Table 1), which is used as the baseline for the sensitivity analysis in Section 4.4. The H_2 power conversion components — i.e., electrolyzer and fuel cell — are lower capacity than LIB charge/discharge power, whereas H_2 energy storage capacity is significantly larger than LIB energy storage capacity. Furthermore, there is significant oversizing of the wind farm, with the maximum wind farm power of 84 MW far exceeding the maximum electrical power demand of 32.7 MW. The annualized cost of the microgrid is USD $43.3 million, of which each subsystems accounts for a meaningful share.

4.2 Operation

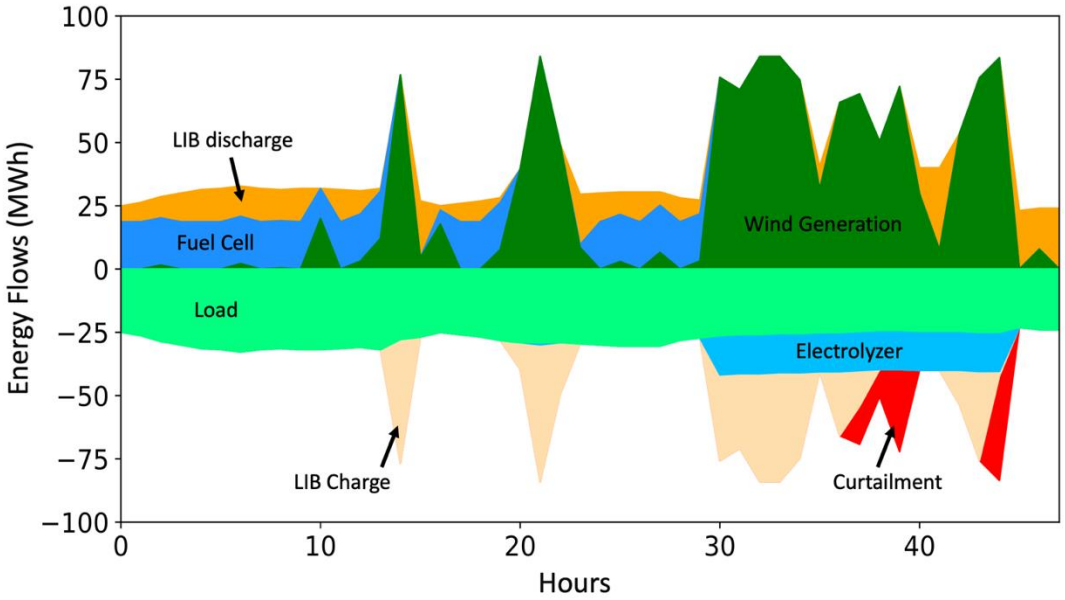

Figure 2: Hourly Energy Flows Through All Components of the Microgrid (First 48 Hours of the 2020 Hybrid Base Case). Positive values correspond to energy supply, and negative values correspond to energy consumption.

Figure 2 illustrates how the system operates hour-to-hour in the *2020 Hybrid Base Case*. The full set of data for the entire year can be found in the supplementary table. It can be observed that the energy produced (wind generation + LIB discharge + fuel cell) and used (load + LIB charge + electrolyzer + curtailment) are in balance. When the wind power generation is lower than the load (i.e., electricity power demand), the fuel cell and LIB (discharge) produce energy to cover the difference. When wind power generation exceeds the load, excess energy is directed to the electrolyzer and LIB. Energy is curtailed when the energy storage systems are at their full capacity but there is still excess wind power, or when the wind power exceeds the sum of the LIB charging capacity and the electrolyzer power capacity.

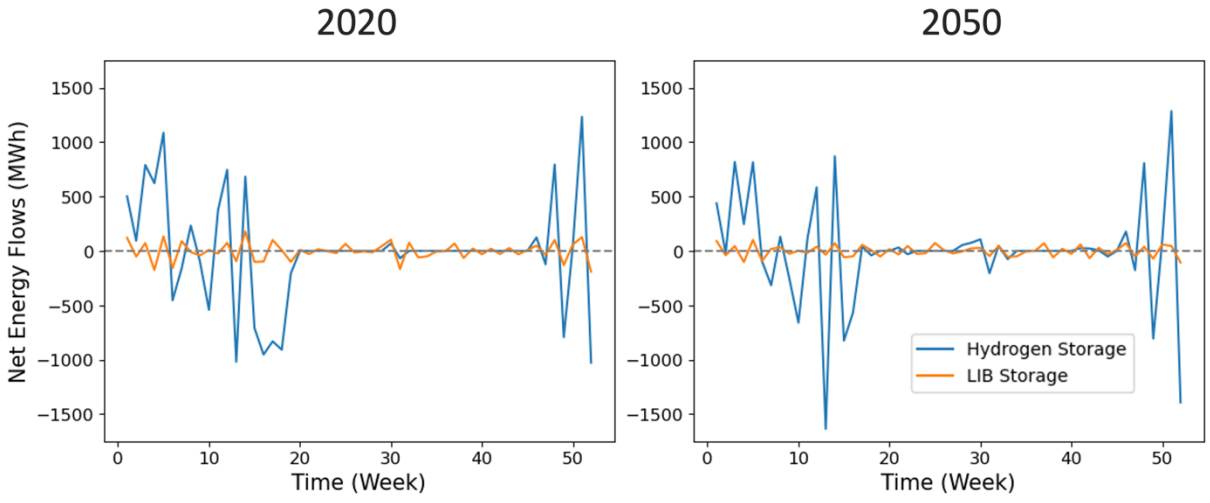

Figure 3: Weekly Net Energy for the H_2 and LIB Subsystems. Net energy is calculated as the sum of energy entering into storage (after efficiency losses) minus energy leaving storage (before efficiency losses). Values above zero indicate that H_2 or LIB is supplying energy to the system.

As seen in Figure 3, there are extended multi-week periods of positive or negative energy flows for the H_2 subsystem. These periods correspond to periods of under/over-generation of wind power relative to the load (see Appendix XXX) — in particular, there are periods of deficit at the beginning and end of year (i.e., winter), with the stable middle period (i.e., summer) corresponding to wind overgeneration and a full H_2 storage. In contrast, the net weekly energy flow of the LIB subsystem does not display obvious seasonal variation. This clearly illustrates that the H_2 subsystem is better suited to address seasonal energy storage requirements, whereas the LIB subsystem is more effective for short-term energy balancing. The weekly operating profiles of the LIB and H_2 subsystems change only slightly from 2020 to 2050 while displaying the same seasonal patterns.

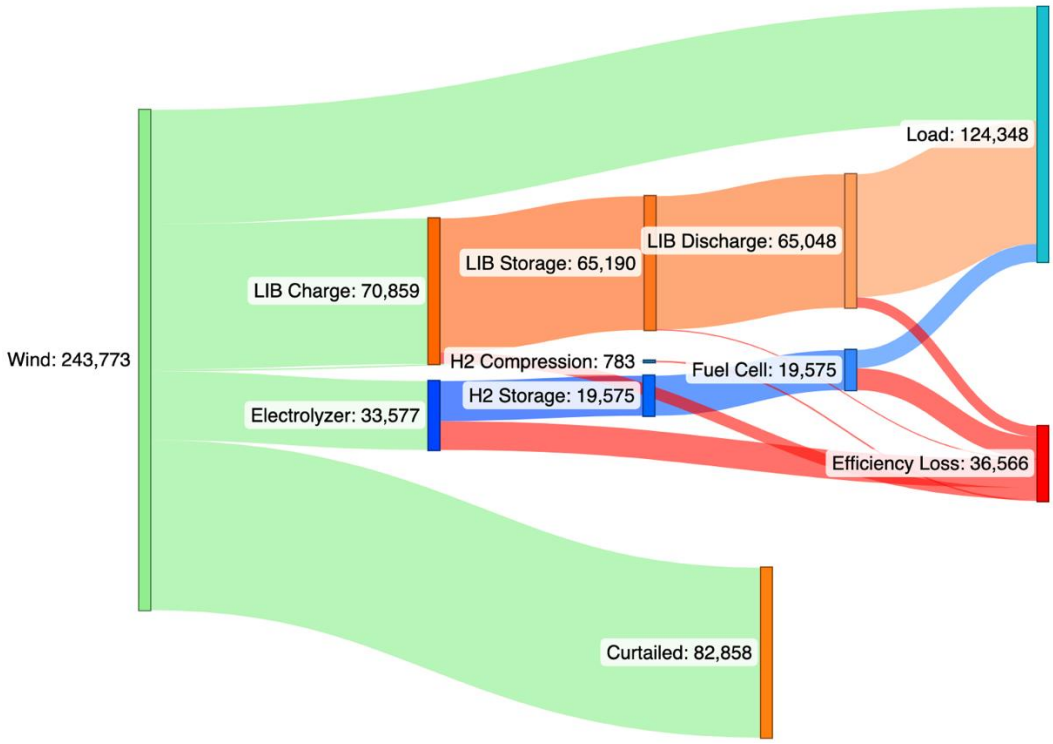

Figure 4: Annual Energy Flows, 2020 Hybrid Base Case. Unit is MWh. Total generation is 196% of the load, and 49% of all generation is either curtailed (34%) or lost due to conversion/storage efficiency (15%). Load is met roughly equally by the wind electricity directly (55%) and energy storage (45%). The LIB subsystem accounts for 88% of the load met by energy storage and receives 68% of the wind electricity directed to energy storage.

Figure 4 shows the energy flow of the microgrid under the *2020 Hybrid Base Case*. Slightly more load is met using energy storage than is met directly by wind electricity. Comparing the two energy-storage subsystems, substantially more of the load is met by LIB than H_2 (88% vs. 12%), despite the LIB subsystem accounting for a slightly smaller portion of the microgrid cost (see Table 3). The higher energy throughput for LIB reflects the fact that the LIB subsystem is constantly cycling on an hourly/daily timescale to balance the system, whereas the H_2 subsystem is employed to cover seasonal demand-supply bottlenecks (see Table 4). This illustrates the extra value in when/over what timescales H_2 is able to provide energy, as well as the importance of LIB for daily balancing. Annual flows for the 2050 Case can be found in Figure S__.

*Table 4: Annual Operation Data, 2020 Hybrid Base Case and 2050 Hybrid Case. The top half of the table reports total operating hours and the share of the year that each component (plus wind curtailment) was active. The bottom half reports the gross annual electricity throughput and annual capacity factor of each component. LIB charge/discharge and electrolyzer totals are the electricity inputs (since their capacity is defined by power input) and fuel cell is the electricity output. Capacity factors were calculated by dividing annual energy by component capacity * number of hours in a year.*

	2020	**2050**	**2020**	**2050**
Operating Hours	Total	Total	Share of Year (%)	Share of Year (%)
Electrolyzer	2,404	2,125	27.4%	24.3%
Fuel Cell	7,08	1,742	8.1%	19.9%
LIB Charge	3,992	3,769	45.6%	43.0%
LIB Discharge	4,598	4,111	52.5%	47.4%
Wind	6,548	6,548	74.7%	74.7%
Curtailment	3,023	2,110	34.5%	24.1%
Annual Capacity Factor	Total (MWh)	Total (MWh)	Capacity Factor (%)	Capacity Factor (%)
Electrolyzer	33,577	41,181	25.4%	20.3%
Fuel Cell	8,809	20,691	5.4%	10.7%
LIB Charge	70,859	48,211	14.9%	18.6%
LIB Discharge	65,048	45,731	13.7%	17.6%
Wind	243,774	203,145	33.1%	33.1%
Curtailment	82,858	52,266	~	~

The LIB subsystem operates for significantly more hours of the year than H_2 components in both 2020 and 2050. By summing up the charging and discharging hours of the LIB subsystem in Table 4, we can see that the LIB subsystem runs 98.1% of the time under the 2020 base case. However, the LIB subsystem has a low annual capacity factor of 28.6% (sum of charging and discharging), which is similar to that of the H_2 subsystems in the 2020 base case. This indicates that the LIB subsystem is charging and discharging more frequently but at lower capacities to balance daily energy mismatches, whereas the H_2 subsystem operates less frequently but at higher capacities to cover weekly/seasonal mismatches.

Hours of operation and capacity factors for both the LIB and H_2 subsystems are similar in the 2020 and 2050 cases, except for the fuel cell which operates significantly more frequently and at higher capacity in 2050. However, the total energy throughput of each system changes significantly. Compared to the 2020 base case, energy directed towards LIB charging and discharging decreases by roughly half in the 2050 case, whereas total energy input to electrolyzer and fuel cell increases by 25% and 138%, respectively. This is due to the technological improvements in the components in the H_2 subsystem. Nevertheless, the LIB subsystem will continue to play an important role in frequent, intra-day energy balancing, but H_2 receives and supplies more energy, possibly to make up for greater seasonal mismatches resulting from the lower wind generation capacity in the 2050 case, and possibly because lower costs and higher power conversion efficiencies enable H_2 to provide more short/mid-duration functionality.

4.3 Core Cases Cost Comparisons

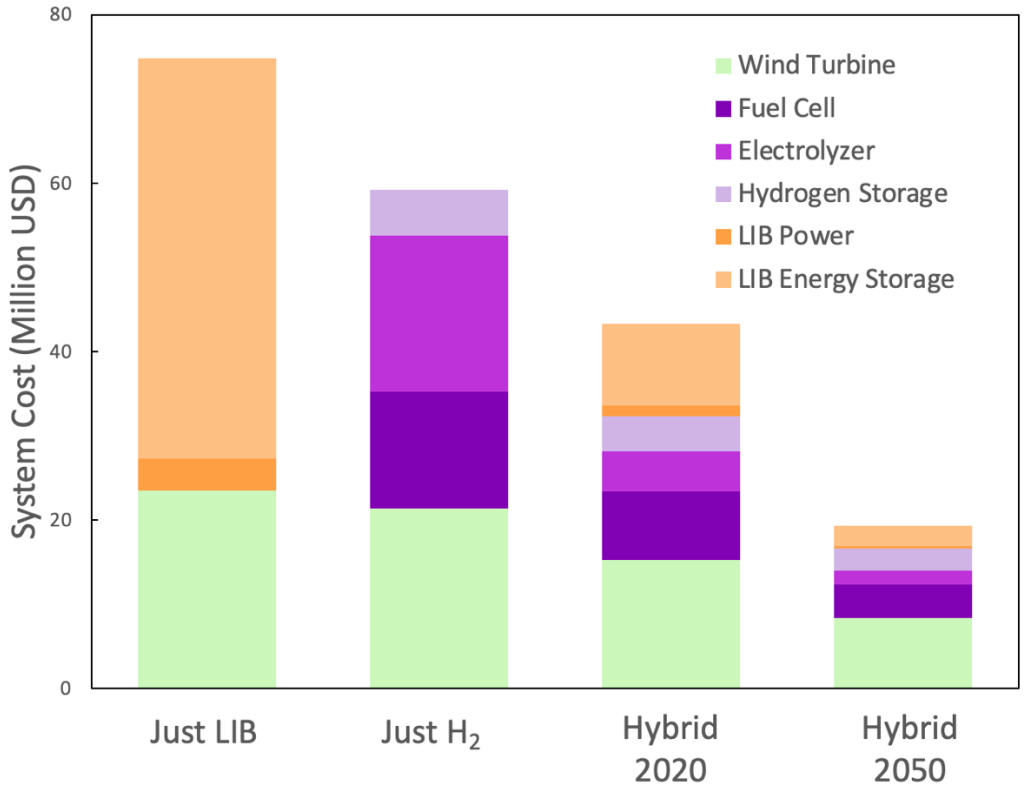

Figure 5: Annualized Cost Breakdown for Core Cases. 'Just LIB' refers to a microgrid that uses only LIB for energy storage (i.e., just LIB power and LIB energy storage components) with 2020 cost and efficiency parameters; 'Just H_2' refers to using only H_2 for energy storage (i.e., comprised of electrolyzers and fuel cells for power conversion and tanks for storage); '2020' is the baseline hybrid system described in section 4.1; '2050' is the hybrid system assuming 2050 cost and efficiency targets/projections are achieved.

To identify the cost benefits of hybridizing LIB and H_2 energy storage, we also studied the costs of the microgrids with only one storage technology, i.e., Just LIB or Just H_2 cases, using the costs and efficiencies of the 2020 base case. Compared to *Just LIB* or *Just H_2*, the hybrid system provided significant cost reductions (see Figure 5). Relying on only LIB for energy storage ($74.8 million) was more expensive than relying on only H_2 ($59.2 million), and significantly more expensive than the hybrid case ($43.3 million). The overall energy storage system accounts for the majority of cost in both *Just LIB* and *Just H_2* systems — 68.6% for *Just LIB* and 63.9% for *Just H_2*, while the renewable generation subsystem costs are similar in both cases (31.4% and 36.1%). In the *Just LIB* case, LIB energy storage capacity drives costs (63.6%), whereas power conversion capacity (i.e., the fuel cell and electrolyzer) drives costs in the *Just H_2* case (54.7%). This is because LIB energy storage capacity is expensive, resulting in high system costs when LIB energy storage capacity is sized to store large quantities of energy over seasonal timescales. In contrast, H_2 storage capacity costs are relatively low but power conversion capacity costs (i.e., electrolyzer and fuel cell) are high, so relying on H_2 to provide all short-duration demand balancing is similarly inefficient.

The microgrid in the *2020 Hybrid Base Case* required less expenditure on both wind generation and energy storage than either *Just LIB* or *Just H_2*. And costs are nearly evenly distributed among the wind farm, the H_2 system (including both conversion and storage), and the LIB system.

We also analyzed a future microgrid with hybrid LIB-H_2 energy storage based on predicted technological advancements and targets. By 2050, the cost of the hybrid-storage microgrid falls by 55.4%

to $19.1 million. The cost distribution between the energy storage and wind farm remains similar —65:35 and 57:43 in 2020 and 2050, respectively. However, the H_2 subsystem accounts for a greater share of the cost of the energy storage system in 2050 compared to 2020 (74.9% versus 60.8%) and a much greater share of total microgrid cost (42.5% versus 14.2%). This confirms that going forward, hydrogen can play a significant role in a hybrid LIB-H_2 microgrid but will not completely displace LIB as an important energy storage option.

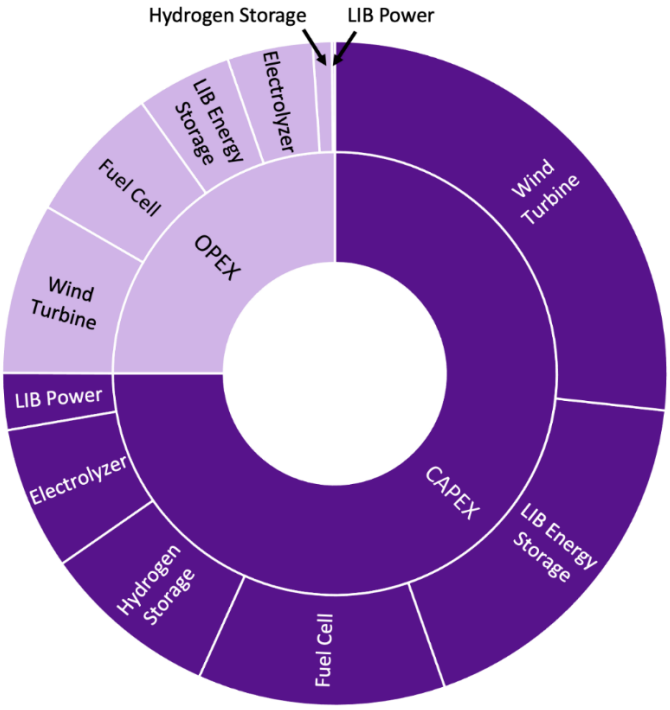

Figure 6: Breakdown of Annualized Cost Between CAPEX and OPEX, 2020 Hybrid Base Case

Figure 6 shows the breakdown of the annualized CAPEX and OPEX of the *2020 Hybrid Base Case*. CAPEX accounted for 75% of total annualized microgrid cost. Among all the components, the wind farm accounted for the greatest share of CAPEX (35.7%). Within the hybrid energy system, LIB energy storage accounted for a greater share of total CAPEX than any other single storage component — 24%, compared with 16.4%, 11.5%, 9.3% for fuel cell, H_2 storage, and electrolyzer, respectively. However, altogether, the H_2 subsystem (36.9%) accounted for a greater share of microgrid CAPEX than the LIB subsystem (27.5%). Regarding OPEX, the operation of the wind farm accounted for the greatest share of any single component, while the H_2 sub-system has a significantly higher OPEX than the LIB sub-system.

4.4 Sensitivity Analysis

In this section, results from the sensitivity analysis using the *2020 Hybrid Base Case* will be presented to identify the technological parameters that have the greatest impact on the microgrid cost and configuration.

4.4.1 Sensitivity of Total Microgrid Cost to Component Technology Cost

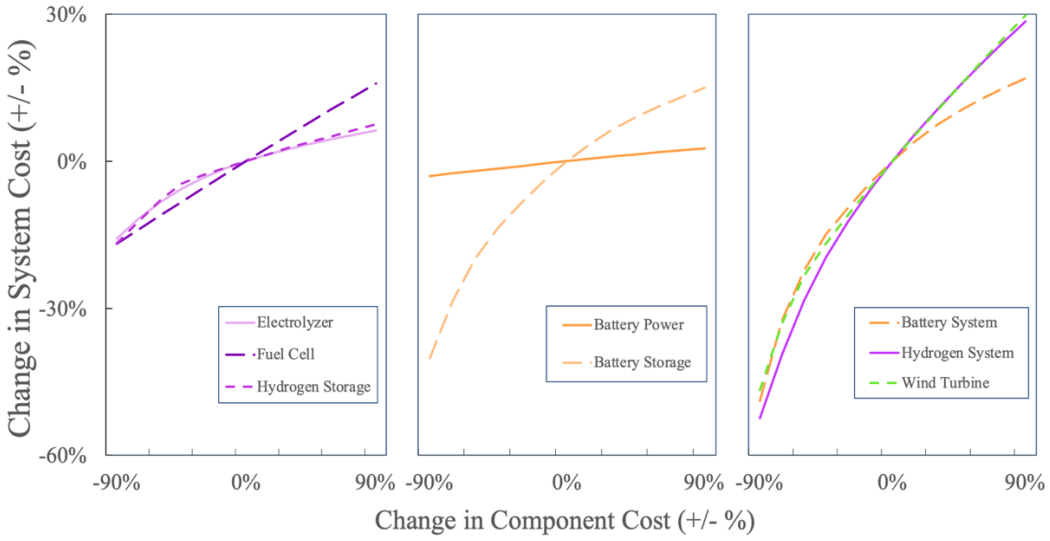

Figure 7: Impact of the Cost of Different Technologies and Subsystems on Total Microgrid Cost. Components of the H_2 subsystem (left); Components of the LIB subsystem (middle); energy storage and wind farm subsystems (right). To change subsystem cost, the annualized cost of each technology in the subsystem was changed by the same percentage.

The total cost of the microgrid is similarly sensitive to each subsystem (the LIB and H_2 subsystems and the wind farm) with the exception that higher LIB subsystem costs have a lower impact than increases in wind farm or H_2 subsystem costs (Figure 7, right). Currently, the components of the H_2 subsystem are less commercially mature than those of the LIB subsystem and wind farm. However, with the manufacturing scaling up, there may be higher potential to reduce the costs of fuel cells, electrolyzers and H_2 storage, which will reduce total microgrid costs.

The impact of the LIB subsystem on the total system cost is driven by the cost of energy storage capacity ($/kWh). As shown in the middle panel of Figure 7, the cost of LIB power conversion capacity ($/kW) has a negligible impact on system cost, while the system cost varies significantly with the cost of LIB energy storage capacity. At -90% and +90% LIB power conversion capacity costs, the cost of the microgrid changes by -3% and +2.6%, respectively. In contrast, the impact of LIB energy storage capacity cost on the microgrid cost ranges between 40.2% and +15%. Furthermore, reducing LIB energy capacity cost yields increasing marginal returns; in other words, continued reductions yield increasing benefits.

The component technologies of the H_2 subsystem have similar impacts on the microgrid cost. When the unit costs of the fuel cell, electrolyzer, and H_2 storage are reduced by 90%, the microgrid cost decreases by 16.2%, 15.8%, and 16.7%, respectively (Figure 7, left panel). However, the intermediate gains from reducing fuel cell cost are greater than electrolyzer and H_2 storage. Reducing fuel cell cost by 45% reduced total microgrid cost by 8.3%, compared to 5.7% for the electrolyzer and 4.6% for H_2 storage. Increased fuel cell cost had a greater impact than increases in electrolyzer or energy storage costs — +15.9%, +6.3%, and +7.5%, respectively. Overall, lowering the costs of each component in the H_2 subsystem has similar potential to reduce the overall cost of the microgrid.

4.4.2 Sensitivity of Total Microgrid Cost to Component Efficiency

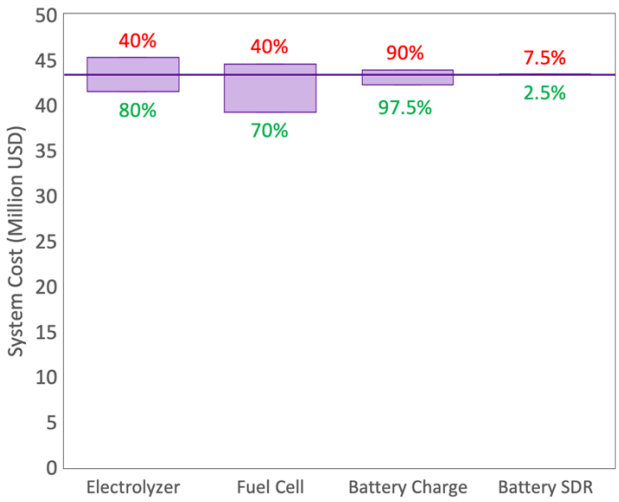

Figure 8: Impact of Component Efficiency/Self-Discharge Rate (SDR) on Total System Cost. Efficiency ranges for each technology reflect the lowest current estimates and targeted future efficiencies. The solid line is the baseline system cost from the 2020 Hybrid Base Case. Note that little attention in the literature is given to battery self-discharge rate. Here, we scale a standard assumption of 5% monthly SDR by ±50%, giving a range of 2.5%-7.5%.

We analyzed how the performances of each component in the hybrid energy storage affect the overall microgrid costs under optimistic and pessimistic scenarios. The optimistic performances were assumed to be the targeted efficiency in 2050, while the pessimistic scenarios were taken from the lower performances of current available technologies. These numbers are summarized in Table S2. Figure 8 illustrates that varying the electrolyzer or battery charging efficiencies has a modest impact on the microgrid cost. However, higher fuel cell efficiency can significantly reduce microgrid costs. At the 2050 target fuel cell efficiency of 70%, the microgrid cost is reduced to $39.2 million. Decreasing electrolyzer efficiency to the 2020 low estimate of 40% resulted in the greatest increase in system cost to $45.3 million. The efficiency of the H_2 system components (electrolyzer and fuel cell) had a greater impact than the LIB system. LIB charge/discharge and LIB monthly self-discharging rate had negligible effects of system cost.

4.5 Impact of Cost on Microgrid System Composition

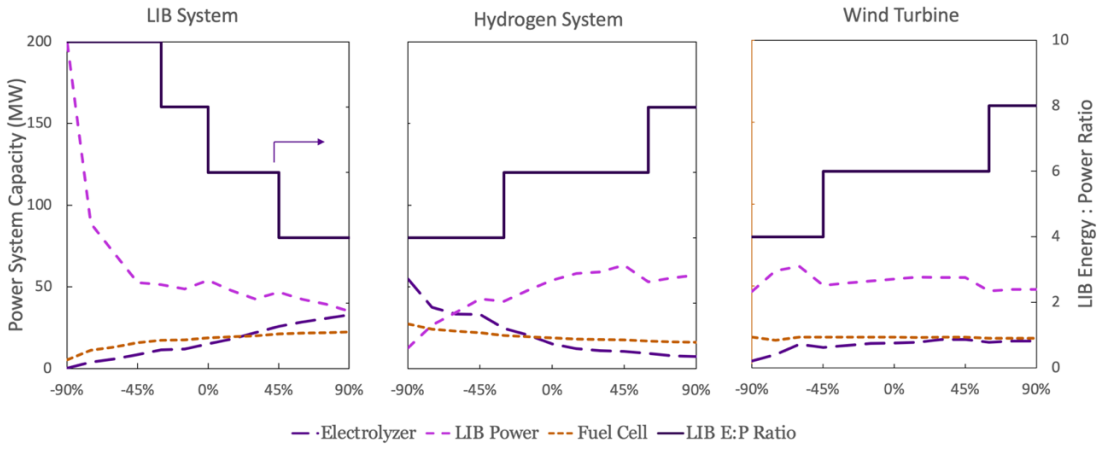

Figure 9: Impact of Subsystem Costs on Component Sizing and the LIB Energy-Power. The left, middle, and right graphs show the impact of LIB subsystem, H_2 subsystem, and wind turbine cost on system composition,

respectively. To change subsystem cost, the annualized cost of each component of the subsystem was changed by the same percentage. Dashed lines are the power conversion components, and the solid line is the LIB energy-power ratio.

As shown in Figure 9, the composition of the hybrid LIB- H_2 storage (i.e., component capacities) is sensitive to the cost of the LIB and H_2 subsystems, and relatively insensitive to the cost of the wind farm. Electrolyzer capacity is inversely correlated with LIB subsystem cost, and LIB power and energy capacity are inversely correlated with H_2 subsystem cost. Fuel cell capacity is relatively stable except when the LIB system is highly discounted. Wind turbine cost has a limited impact on the composition of storage, with the exception that highly discounted wind turbines result in very low electrolyzer capacity, likely because there is greater energy surplus from more wind electricity production that can be captured at lower capacity over more hours instead of requiring higher capacity during fewer hours. Regarding storage, the LIB energy-power ratio decreases as the LIB subsystem gets more expensive and increases as the H_2 subsystem and wind turbines get more expensive. This suggests that as the H_2 subsystem and wind farm get cheaper, the LIB subsystem specializes more in providing short-duration storage.

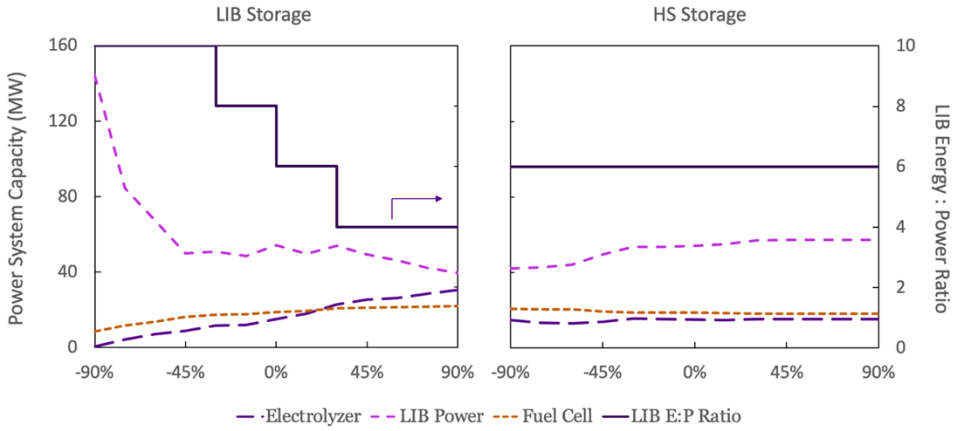

Figure 10: Impact of Energy Storage Technology Cost on Sizing and LIB Energy-Power Ratio. The x-axis displays percentage change in annualized energy storage capacity cost in $/kWh. The left and right panels show the impact of LIB and H_2 energy storage capacity costs on system composition, respectively. Dashed lines are the power conversion components, and the solid line is the LIB energy-power ratio.

Energy is stored in the LIB or H_2 tanks. System composition is sensitive to LIB energy storage capacity costs and insensitive to H_2 storage costs. As discussed in sections 4.1 and 4.3, LIB energy storage capacity accounts for most of the LIB subsystem cost, suggesting that energy storage capacity cost is the primary constraint on LIB subsystem sizing. Figure 10 (left panel) shows that as this constraint is relaxed, both LIB power conversion capacity and the ratio of LIB energy-to-power increases. Thus, as LIB energy storage capacity becomes cheaper, the LIB subsystem provides energy storage over longer durations. Similarly, LIB energy storage costs are inversely correlated with electrolyzer and fuel cell capacity, meaning that reductions in LIB energy storage capacity cost enable LIB to partially displace the H_2 subsystem. Note that the impact on microgrid composition is modest up until a 45% decrease in LIB energy storage capacity cost, after which the LIB power conversion capacity grows significantly, indicating a possible tipping point to use LIB for longer-term energy storage.

In contrast, H_2 energy storage capacity cost has almost no impact on microgrid system composition when its cost changes between -90% and +90% of the *2020 Hybrid Base Case* value. The LIB energy-power ratio is the same across the range of the sensitivity analysis, indicating that the LIB subsystem's role is largely unchanged by H_2 energy storage capacity costs. Fuel cell and electrolyzer

capacities are the same when H_2 energy storage cost changes in a wide range, suggesting that H_2 energy storage capacity costs impose little constraint on the sizing of the H_2 power conversion components.

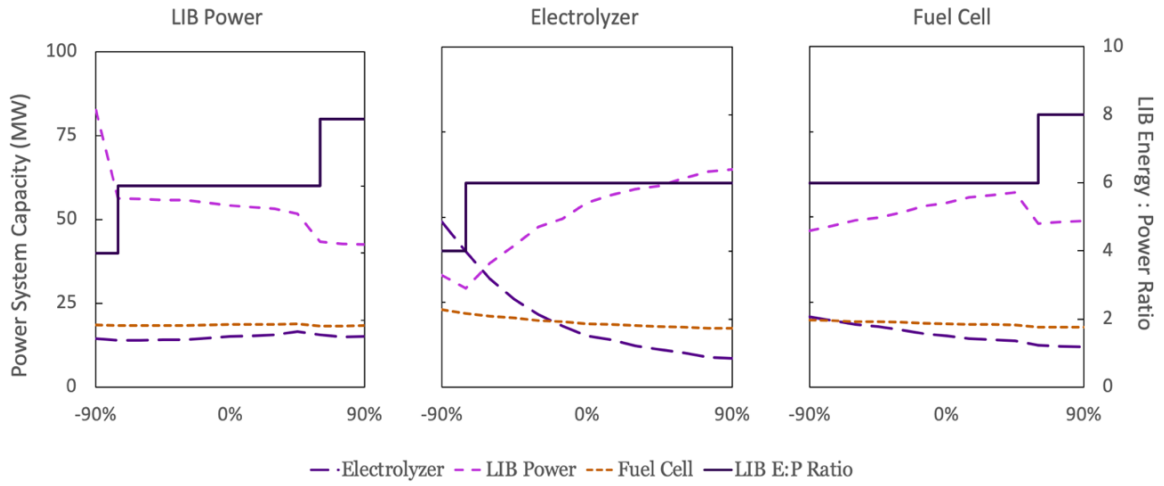

Figure 11: Impact of Power Conversion Technology Cost on Sizing and LIB Energy-Power Ratio. The x-axis displays percentage change in annualized power conversion cost in $/kW. The left, middle, and right panels show the impact of LIB power conversion (i.e., charge and discharge), electrolyzer, and fuel cell cost on system composition, respectively. Dashed lines are the power conversion components, and the solid line is the LIB energy-power ratio.

As the cost of LIB power conversion changes (Figure 11, left panel), only the LIB power conversion and energy storage capacities are impacted. LIB power conversion capacity is relatively stable as its unit cost changes, except once a certain threshold is passed and the LIB energy-power ratio changes, which causes LIB power conversion capacity to sharply increase or decrease. This shows that LIB energy storage capacity is likely constraining LIB power conversion capacity.

As the unit cost of the electrolyzer decreases (Figure 11, middle panel), electrolyzer capacity displaces a certain portion of LIB power conversion capacity. This is in contrast with the trend observed in the left panel of Figure 11, which shows that cheaper LIB power conversion does not result in lower electrolyzer capacity. Fuel cell's unit capacity cost has a limited impact on the composition of the hybrid storage (Figure 11, right panel). The fact that fuel cell capacity is relatively constant across all sensitivity analyses and changing fuel cell capacity cost itself has little impact, suggests that the fuel cell is sized according to an operational bottleneck when there is a maximum deficit between the power demand and the wind farm power output.

5 Conclusion

Microgrids enable the deployment of renewables with reduced need for new transmission and distribution infrastructure. For microgrids with high shares of renewables, hybridizing LIB and H_2 storage can resolve issues of renewable variability/intermittency across multiple timescales. In this paper, we developed a SL-MILP model to study a wind-supplied microgrid with hybrid LIB-H_2 storage to 1) compare the cost benefits of a hybrid LIB-H_2 storage technology versus using a single storage, 2) study the operation of a microgrid with hybrid storage, and 3) conduct sensitivity analyses on the impact of component cost and efficiency on system cost and composition. The conclusions are:

- The LIB and H_2 systems fulfill distinct energy storage functions. The LIB system operates for more hours a year and at lower capacity factors and displays little seasonal variation. The H_2

system provides significantly less total energy and operates over fewer hours, despite accounting for a slightly higher share of cost, illustrating the value H_2 provides by supply energy during seasonal bottlenecks.

- Energy storage plays a substantial role in system operation. More than half of load is met using energy storage, which coincides with significant overgeneration and curtailment of wind, as well as efficiency losses. Overgeneration, curtailment, and efficiency losses decline substantially by 2050, while the role of energy storage increases.
- Compared to the 2020 base case, in 2050 the H_2 subsystem receives/supplies significantly more energy, likely because lower wind farm capacity exacerbates seasonal demand-supply bottlenecks requiring more long-duration storage. The LIB subsystem receives/supplies less energy and operates fewer hours. However, LIB's capacity factor increases, and the LIB subsystem continues to play an important role in frequent intra-day balancing.
- Neither LIB nor H_2 storage alone achieve minimum cost for a 100%-wind supplied microgrid. A hybrid-storage system offers significant cost reductions. In the 2020 baseline hybrid-storage microgrid, total cost is distributed evenly among the three subsystems— H_2, LIB, and the wind farm. Going forward, achieving 2050 cost and efficiency targets will reduce the LIB-H_2 system cost by more than half compared to the 2020 baseline, and H_2's share of system cost increases while LIB's share decreases.
- The cost of the microgrid is similarly sensitive to the cost of H_2, LIB, and the wind farm subsystems. Each component of the H_2 subsystem — fuel cell, electrolyzer, and H_2 storage tanks— have a meaningful impact on system cost. In contrast, the impact of LIB subsystem is dominated by the cost of LIB energy storage.
- Achieving 2050 efficiency projections/targets fuel cell has the greatest impact on system cost of possible efficiency improvements. Conversely, at the 2020 low-efficiency range, electrolyzers cause the greatest increase in system cost. The effects of LIB charge/discharge efficiency and self-discharge rate are limited.
- System composition is sensitive to cost of LIB and H_2 but not wind. LIB displaces H_2 only when LIB energy storage costs decrease, whereas H_2 displaces LIB primarily when electrolyzer unit costs decrease. Fuel cell and H_2 storage costs have limited impact on system composition, and fuel cell capacity remains fairly constant across the sensitivity cases.

Declaration of interests

The authors declare no competing interests.

Acknowledgement

This work was supported by the Departments of Mechanical and Mechatronics Engineering at the University of Waterloo and was made possible by the facilities of the Shared Hierarchical Academic Research Computing Network (SHARCNET) and the Digital Research Alliance of Canada. We acknowledge the support of the Natural Sciences and Engineering Research Council of Canada (NSERC), [funding reference number RGPIN-2021-02453]. We would like to thank Lucas Wen Tang and Ryan Quan for generating the residential electricity demand profile.

6 Work Cited

[1] Energy Sector Management Assistance Program, *Mini Grids for Half a Billion People*. World Bank, Washington, DC, 2019. doi: 10.1596/31926.

[2] U.S. Department of Energy, "Microgrid and Integrated Microgrid Systems Program Report," Office of Electricity, 050922, Jan. 2022.

[3] A. Ali, W. Li, R. Hussain, X. He, B. Williams, and A. Memon, "Overview of Current Microgrid Policies, Incentives and Barriers in the European Union, United States and China," *Sustainability*, vol. 9, p. 1146, Jun. 2017, doi: 10.3390/su9071146.

[4] W. Feng *et al.*, "A review of microgrid development in the United States – A decade of progress on policies, demonstrations, controls, and software tools," *Appl. Energy*, vol. 228, pp. 1656–1668, Oct. 2018, doi: 10.1016/j.apenergy.2018.06.096.

[5] J. A. Yarmuth, "Text - H.R.5376 - 117th Congress (2021-2022): Inflation Reduction Act of 2022," Aug. 16, 2022. http://www.congress.gov/ (accessed Dec. 16, 2022).

[6] Energy Sector Management Assistance Program, "Mini Grids for Half a Billion People: Market Outlook and Handbook for Decision Makers," World Bank, Washington, DC, Technical Paper, Jun. 2019. doi: 10.1596/31926.

[7] N. Awofeso, "Generator Diesel Exhaust: a Major Hazard to Health and the Environment in Nigeria," *Am. J. Respir. Crit. Care Med.*, vol. 183, no. 10, pp. 1437–1437, May 2011, doi: 10.1164/ajrccm.183.10.1437.

[8] S. Canada, "A healthy environment and a healthy economy," Feb. 12, 2021. https://www.canada.ca/en/services/environment/weather/climatechange/climate-plan/climate-plan-overview/healthy-environment-healthy-economy.html (accessed Aug. 09, 2022).

[9] J. J. Hargreaves and R. A. Jones, "Long Term Energy Storage in Highly Renewable Systems," *Front. Energy Res.*, vol. 8, 2020, Accessed: Jul. 28, 2022. [Online]. Available: https://www.frontiersin.org/articles/10.3389/fenrg.2020.00219

[10] K. Santos-Pereira, J. Pereira, L. Veras, D. Cosme, D. Oliveira, and O. Saavedra, "The requirements and constraints of storage technology in isolated microgrids: a comparative analysis of lithium-ion vs. lead-acid batteries," *Energy Syst.*, May 2021, doi: 10.1007/s12667-021-00439-7.

[11] "Green hydrogen cost reduction: Scaling up electrolysers to meet the 1.5C climate goal," p. 106.

[12] D. S. Satyapal, "U.S. Department of Energy Hydrogen and Fuel Cell Technologies Office Overview," *Renew. ENERGY*.

[13] "Hydrogen Shot," *Energy.gov*. https://www.energy.gov/eere/fuelcells/hydrogen-shot (accessed Aug. 10, 2022).

[14] "How the Inflation Reduction Act of 2022 Will Advance a U.S. Hydrogen Economy," *Fuel Cell & Hydrogen Energy Association*. https://www.fchea.org/transitions/2022/8/5/how-the-inflation-reduction-act-of-2022-will-advance-a-us-hydrogen-economy (accessed Aug. 10, 2022).

[15] *COMMUNICATION FROM THE COMMISSION TO THE EUROPEAN PARLIAMENT, THE EUROPEAN COUNCIL, THE COUNCIL, THE EUROPEAN ECONOMIC AND SOCIAL COMMITTEE AND THE COMMITTEE OF THE REGIONS REPowerEU Plan*. 2022. Accessed: Aug. 10, 2022. [Online]. Available: https://eur-lex.europa.eu/legal-content/EN/TXT/?uri=COM%3A2022%3A230%3AFIN&qid=1653033742483

[16] "Mid-Longterm Hydrogen Industry Development Goals (2021-2035) - Chinese National Development and Reform Commission." https://www.ndrc.gov.cn/xxgk/zcfb/ghwb/202203/t20220323_1320038.html?code=&state=123 (accessed Aug. 10, 2022).

[17] A. S. Jacob, R. Banerjee, and P. C. Ghosh, "Sizing of hybrid energy storage system for a PV based microgrid through design space approach," *Appl. Energy*, vol. 212, pp. 640–653, Feb. 2018, doi: 10.1016/j.apenergy.2017.12.040.

[18] L. Moretti, M. Astolfi, C. Vergara, E. Macchi, J. I. Pérez-Arriaga, and G. Manzolini, "A design and dispatch optimization algorithm based on mixed integer linear programming for rural electrification," *Appl. Energy*, vol. 233–234, pp. 1104–1121, Jan. 2019, doi: 10.1016/j.apenergy.2018.09.194.
[19] M. A. Hannan, M. Faisal, P. Jern Ker, R. A. Begum, Z. Y. Dong, and C. Zhang, "Review of optimal methods and algorithms for sizing energy storage systems to achieve decarbonization in microgrid applications," *Renew. Sustain. Energy Rev.*, vol. 131, p. 110022, Oct. 2020, doi: 10.1016/j.rser.2020.110022.
[20] A. Chauhan and R. P. Saini, "A review on Integrated Renewable Energy System based power generation for stand-alone applications: Configurations, storage options, sizing methodologies and control," *Renew. Sustain. Energy Rev.*, vol. 38, pp. 99–120, Oct. 2014, doi: 10.1016/j.rser.2014.05.079.
[21] P. Marocco, D. Ferrero, E. Martelli, M. Santarelli, and A. Lanzini, "An MILP approach for the optimal design of renewable battery-hydrogen energy systems for off-grid insular communities," *Energy Convers. Manag.*, vol. 245, p. 114564, Oct. 2021, doi: 10.1016/j.enconman.2021.114564.
[22] B. Li, R. Roche, and A. Miraoui, "Microgrid sizing with combined evolutionary algorithm and MILP unit commitment," *Appl. Energy*, vol. 188, pp. 547–562, Feb. 2017, doi: 10.1016/j.apenergy.2016.12.038.
[23] A. Maleki and F. Pourfayaz, "Optimal sizing of autonomous hybrid photovoltaic/wind/battery power system with LPSP technology by using evolutionary algorithms," *Sol. Energy*, vol. 115, pp. 471–483, May 2015, doi: 10.1016/j.solener.2015.03.004.
[24] M. Zatti *et al.*, "k-MILP: A novel clustering approach to select typical and extreme days for multi-energy systems design optimization," *Energy*, vol. 181, pp. 1051–1063, Aug. 2019, doi: 10.1016/j.energy.2019.05.044.
[25] L. Weimann and M. Gazzani, "A novel time discretization method for solving complex multi-energy system design and operation problems with high penetration of renewable energy," *Comput. Chem. Eng.*, vol. 163, p. 107816, Jul. 2022, doi: 10.1016/j.compchemeng.2022.107816.
[26] L. Kotzur, P. Markewitz, M. Robinius, and D. Stolten, "Impact of different time series aggregation methods on optimal energy system design," *Renew. Energy*, vol. 117, pp. 474–487, Mar. 2018, doi: 10.1016/j.renene.2017.10.017.
[27] "Ontario's Low-Carbon Hydrogen Strategy," *ontario.ca*. http://www.ontario.ca/page/ontarios-low-carbon-hydrogen-strategy (accessed Aug. 10, 2022).
[28] U. Wilke, F. Haldi, J.-L. Scartezzini, and D. Robinson, "A bottom-up stochastic model to predict building occupants' time-dependent activities," *Build. Environ.*, vol. 60, pp. 254–264, Feb. 2013, doi: 10.1016/j.buildenv.2012.10.021.
[29] "Survey data | Centre for Time Use Research." https://www.timeuse.org/survey-data (accessed Dec. 22, 2022).
[30] "eQUEST." https://www.doe2.com/equest/ (accessed Dec. 22, 2022).
[31] "Residential Electricity and Natural Gas Plans," *EnergyRates.ca*. https://energyrates.ca/residential-electricity-natural-gas/ (accessed Dec. 22, 2022).
[32] "Toronto Historical Wind Speed," *Amateur Weather Statistics for Toronto, Ontario*. https://toronto.weatherstats.ca/metrics/wind_speed.html (accessed Dec. 27, 2022).
[33] S. Haas *et al.*, "wind-python/windpowerlib: Silent Improvements." Zenodo, Mar. 09, 2021. doi: 10.5281/zenodo.4591809.
[34] "2021 CMTS," *Tableau Software*. https://public.tableau.com/views/2021CMTS/TechSummary?:embed=y&Technology=Utility-Scale%20Battery%20Storage&:embed=y&:showVizHome=n&:bootstrapWhenNotified=y&:apiID=handler0 (accessed Aug. 16, 2022).
[35] "The Future of Energy Storage," *Main*. https://energy.mit.edu/research/future-of-energy-storage/ (accessed Aug. 15, 2022).

[36] O. J. Guerra, J. Eichman, J. Kurtz, and B.-M. Hodge, “Cost Competitiveness of Electrolytic Hydrogen,” *Joule*, vol. 3, no. 10, pp. 2425–2443, Oct. 2019, doi: 10.1016/j.joule.2019.07.006.
[37] Weidner, E., Ortiz Cebolla, R., and Davies, J., “Global deployment of large capacity stationary fuel cells: Drivers of, and barriers to, stationary fuel cell deployment.” European Commission Joint Research Centre, 2019.
[38] T. Ramsden, B. Kroposki, and J. Levene, “Opportunities for Hydrogen-Based Energy Storage for Electric Utilities,” Washington, DC: National Hydrogen Association (NHA), NREL/CP-560-43056, Jan. 2008. Accessed: Aug. 16, 2022. [Online]. Available: https://www.osti.gov/biblio/1346937-opportunities-hydrogen-based-energy-storage-electric-utilities
[39] L. Gracia, P. Casero, C. Bourasseau, and A. Chabert, “Use of Hydrogen in Off-Grid Locations, a Techno-Economic Assessment,” *Energies*, vol. 11, no. 11, Art. no. 11, Nov. 2018, doi: 10.3390/en11113141.
[40] “USD Inflation Calculator - US Dollar (2016-2022).” https://www.inflationtool.com/us-dollar?amount=100&year1=2016&year2=2020&frequency=yearly (accessed Dec. 30, 2022).
[41] M. Penev, C. Hunter, and J. Eichman, “Energy Storage: Days of Service Sensitivity Analysis.” National Renewable Energy Laboratory, May 19, 2019.
[42] D. Feldman, V. Ramasamy, R. Fu, A. Ramdas, J. Desai, and R. Margolis, “U.S. Solar Photovoltaic System and Energy Storage Cost Benchmark: Q1 2020,” *Renew. Energy*, p. 120, 2021.
[43] T. Stehly and P. Duffy, “2020 Cost of Wind Energy Review,” *Renew. Energy*, p. 77, 2022.
[44] “Net Present Cost.” https://www.homerenergy.com/products/pro/docs/latest/net_present_cost.html (accessed Dec. 28, 2022).